Int. J. Heat Mass Transfer. Vol. 28, No. 5, pp. 959–968, 1985
Printed in Great Britain

0017-9310/85 $3.00 + 0.00

Mixed convection about a rotating sphere

R. RAJASEKARAN and M. G. PALEKAR
Department of Mathematics, Indian Institute of Technology, Powai, Bombay 400 076, India

(*Received* 23 *September* 1982 *and in final form* 26 *March* 1984)

Abstract—The paper presents a theoretical analysis of flow and heat transfer characteristics of the effects of buoyancy force on laminar boundary layer over a rotating sphere in forced flow under two kinds of heating conditions: uniform wall temperature and uniform surface heat flux. By applying appropriate coordinate transformations and using Merk's types of series, the governing momentum and energy equations are reduced to a set of coupled ordinary differential equations, which depend on wedge, rotation and buoyancy parameters. Numerical computations are carried out for Prandtl numbers 0.7, 1.0 and for various values of buoyancy and rotation parameters. For aiding flow, it is found that both the friction factor and the local Nusselt number increase with increasing buoyancy force. The local free stream velocity increases with buoyancy which, in turn, affects the friction coefficient and Nusselt number. The coupling between rotation and buoyancy results in increased overshooting of the velocity profiles in the vicinity of the rotating sphere. For an equivalent buoyancy effect, heating by uniform surface heat flux yields larger local Nusselt number than heating by uniform wall temperature. The ratio $Nu_{\mathrm{UHF}}/Nu_{\mathrm{UWT}}$ is higher for the rotating sphere (as compared to a nonrotating case) and further the ratio increases as the sphere spins faster. The effect of free stream, rotation and buoyancy on the eruption of flow is examined and also a suggestion for further investigation is made.

1. INTRODUCTION

IN THE LITERATURE, investigations have been made for laminar heat transfer from rotating axisymmetric round-nosed bodies either for forced convection or for pure convection (see, for example, [1–6]). The density difference arising as a result of temperature difference gives rise to buoyancy force. The neglect of buoyancy effect on forced convective heat transfer may not be justified when the velocity is small and the temperature difference between the surface and the ambient fluid is large. It may be expected that this buoyancy force will affect the momentum and heat transfer rates.

Several authors [7–11] have discussed the effect of buoyancy on non-rotating bodies. For rotating bodies, Lee *et al.* [5] have investigated the laminar boundary-layer transfer in forced flow, neglecting buoyancy force. They have used Merk's [12] types of series modified by Chao [13] and their results compare favourably with previous theoretical and experimental studies. More recently Suwono [6] has considered the problem of buoyancy effects on flow and heat transfer on rotating axisymmetric round-nosed bodies for both aiding and opposing flows in absence of a uniform flow from infinity.

However, it is difficult to clarify the effect of buoyancy force on the flows arising from a combination of rotation and forced flow of comparable magnitude. Such problems arise in the study of re-entry missile behaviour, fibre coating applications, rotary machines etc. The coordinate transformation and Merk's types of series modified by Chao [13] has been employed for the coupled momentum and energy equations. The analysis is carried out for assisting flow (in which the buoyancy force acts in the same direction as the resultant flow due to rotation and flow from infinity) and the behaviour is inferred for opposing flow. The effect of buoyancy on laminar boundary-layer transfer over a rotating sphere in forced flow is investigated.

Chen and Mucoglu considered the problem of mixed convection about a non-rotating sphere under two kinds of heating conditions: (i) uniform wall temperature [5] and (ii) uniform surface heat flux [14]. They concluded that the buoyancy affected velocity profiles exhibit an overshoot beyond the local free stream velocity for aiding flow. Also, for an equivalent buoyancy force effect, heating by UHF yields larger local Nusselt number than heating by UWT. It would be interesting to examine the effect of coupling between the rotation and buoyancy on this phenomenon.

2. GOVERNING EQUATIONS AND SOLUTION METHOD

Consider steady, laminar, non-dissipative, constant property (except the density changes which produce buoyancy forces), incompressible boundary-layer flow around a rotating sphere placed in a uniform stream with its axis of rotation parallel to the free stream velocity and opposite to the gravitational field as depicted in the inset of Fig. 5. Let x, y and z be a non-rotating orthogonal curvilinear coordinate system with the corresponding velocity components u, v and w. If r is the radial distance from a surface element to the axis of symmetry, the governing boundary-layer equations are given by

$$\frac{\partial}{\partial x}(ru)+\frac{\partial}{\partial y}(rv) = 0, \tag{1}$$

$$u\frac{\partial u}{\partial x}+v\frac{\partial u}{\partial y}-\frac{w^2}{r}\frac{\mathrm{d}r}{\mathrm{d}x} = U_e\frac{\mathrm{d}U_e}{\mathrm{d}x} + v\frac{\partial^2 u}{\partial y^2} \pm a\beta(T-T_\infty)\sin\phi \tag{2}$$

NOMENCLATURE

a	acceleration due to gravity
B	rotation parameter $\left(\frac{2}{3}\frac{R\Omega}{u_\infty}\right)^2$ for sphere
C_f	friction coefficient
f	dimensionless stream function
g	dimensionless rotating velocity
Gr	Grashof number, $\frac{a\beta(T_w - T_\infty)R^3}{v^2}$
Gr^*	Grashof number, $a\beta q_w R^4/kv^2$
k	thermal conductivity
Nu	Nusselt number
Pr	Prandtl number, v/α
q_w	local surface heat transfer rate per unit area
r	radius of sphere at x
R	sphere radius
Re_R	Reynolds number, Ru_∞/v
T	temperature
u	velocity component in x direction
u_∞	approach velocity
U_e	velocity at outer edge of boundary layer
UHF	uniform surface heat flux
UWT	uniform wall temperature
v	velocity component in y direction
w	velocity component in rotating direction
x	coordinate measured along surface from stagnation point
y	coordinate measured normal to x
z	coordinate measured in rotating direction.

Greek symbols

α	thermal diffusivity
β	thermal-expansion coefficient
δ_v	velocity boundary-layer thickness
δ_θ	thermal boundary-layer thickness
ϕ	$= x/R$
η	dimensionless y coordinate
θ	dimensionless temperature, $(T-T_\infty)/(T_w-T_\infty)$
λ	buoyancy parameter, Gr/Re_R^2
λ^*	buoyancy parameter, $Gr^*/Re_R^{5/2}$
v	kinematic viscosity
Λ	wedge parameter, $\frac{2\xi}{U_e}\frac{dU_e}{d\xi}$
ξ	dimensionless x coordinate
ψ	stream function
Ω	angular velocity.

Subscripts

w	evaluated at wall
∞	evaluated at approach conditions.

$$u\frac{\partial w}{\partial x} + v\frac{\partial w}{\partial y} + \frac{uw}{r}\frac{dr}{dx} = v\frac{\partial^2 w}{\partial y^2}, \quad (3)$$

$$u\frac{\partial T}{\partial x} + v\frac{\partial T}{\partial y} = \alpha\frac{\partial^2 T}{\partial y^2}. \quad (4)$$

2.1. *Uniform wall temperature*

Here the boundary conditions are

$$\begin{aligned} &u = v = 0, \quad w = \Omega r, \quad T = T_w \quad \text{for } y = 0 \\ &u = U_e, \quad v = w = 0, \quad T = T_\infty \quad \text{for } y \to \infty. \end{aligned} \quad (5)$$

In equation (2), the positive and negative signs are to be taken for assisting and opposing flows respectively. They correspond to the cases $T_w > T_\infty$ and $T_w < T_\infty$ respectively.

The continuity equation is identically satisfied by introducing stream function $\psi(x, y)$ defined by

$$u = \frac{R}{r}\frac{\partial\psi}{\partial y}; \quad v = -\frac{R}{r}\frac{\partial\psi}{\partial x}. \quad (6)$$

The (x, y) coordinate system is transformed into the dimensionless (ξ, η) system according to

$$\xi = \int_0^x \frac{U_e(x)}{u_\infty}\left(\frac{r}{R}\right)^2 \frac{dx}{R}, \quad (7)$$

$$\eta = \left(\frac{Re_R}{2\xi}\right)^{1/2} \frac{U_e}{u_\infty}\left(\frac{r}{R}\right)\frac{y}{R}. \quad (8)$$

$\psi(x, y)$, $w(x, y)$ and $T(x, y)$ are transformed into dimensionless functions f, g and θ as follows

$$\psi(x, y) = u_\infty R\left(\frac{2\xi}{Re_R}\right)^{1/2} f(\xi, \eta), \quad (9)$$

$$w(x, y) = r(x)\Omega g(\xi, \eta), \quad (10)$$

and

$$\theta(\xi, \eta) = \frac{T - T_\infty}{T_w - T_\infty}. \quad (11)$$

Using the above transformations, the momentum and energy equations (2)–(4) with the boundary conditions (5) may be written as

$$f''' + ff'' + \Lambda(1 - f'^2) + \frac{2\xi}{r}\frac{dr}{d\xi}\left(\frac{r^2\Omega^2}{U_e^2}\right)g^2 \pm A\lambda\theta = 2\xi\frac{\partial(f', f)}{\partial(\xi, \eta)}, \quad (12)$$

$$g'' + fg' - \frac{4\xi}{r}\frac{dr}{d\xi}gf' = 2\xi\frac{\partial(g, f)}{\partial(\xi, \eta)}, \quad (13)$$

$$Pr^{-1}\theta'' + f\theta' = 2\xi\frac{\partial(\theta, f)}{\partial(\xi, \eta)}, \quad (14)$$

where

$$A = 2\xi \frac{R^2}{r^2}\left(\frac{u_\infty}{U_e}\right)^3 \sin\phi; \quad \Lambda = \frac{2\xi}{U_e}\frac{dU_e}{d\xi}; \quad \lambda = \frac{Gr}{Re_R^2},$$

with the boundary conditions

$$\begin{aligned} f = f' = 0; \quad g = \theta = 1 \quad &\text{for } \eta = 0 \\ f' = 1; \quad g = \theta = 0 \quad &\text{for } \eta \to \infty. \end{aligned} \tag{15}$$

Now, for a sphere

$$\frac{r}{R} = \sin\phi, \quad \frac{U_e}{u_\infty} = \frac{3}{2}\sin\phi, \quad \frac{4\xi}{r}\frac{dr}{d\xi} = 2\Lambda,$$

$$\frac{2\xi}{r}\frac{dr}{d\xi}\frac{r^2\Omega^2}{U_e^2} = B\Lambda \quad \text{and} \quad A = \frac{8}{27}\frac{(2+\cos\phi)}{(1+\cos\phi)^2}. \tag{16}$$

Following Chao and Fagbenle [13], we write expansions for f, g and θ in the form of Merk's series as

$$f(\xi,\eta) = f_0(\Lambda,\eta) + 2\xi\frac{d\Lambda}{d\xi} f_1(\Lambda,\eta) + 4\xi^2\frac{d^2\Lambda}{d\xi^2} f_2(\Lambda,\eta) + \left(2\xi\frac{d\Lambda}{d\xi}\right)^2 f_3(\Lambda,\eta) + \cdots \tag{17}$$

$$g(\xi,\eta) = g_0(\Lambda,\eta) + 2\xi\frac{d\Lambda}{d\xi} g_1(\Lambda,\eta) + 4\xi^2\frac{d^2\Lambda}{d\xi^2} g_2(\Lambda,\eta) + \left(2\xi\frac{d\Lambda}{d\xi}\right)^2 g_3(\Lambda,\eta) + \cdots \tag{18}$$

$$\theta(\xi,\eta) = \theta_0(\Lambda,\eta) + 2\xi\frac{d\Lambda}{d\xi} \theta_1(\Lambda,\eta) + 4\xi^2\frac{d^2\Lambda}{d\xi^2} \theta_2(\Lambda,\eta) + \left(2\xi\frac{d\Lambda}{d\xi}\right)^2 \theta_3(\Lambda,\eta) + \cdots. \tag{19}$$

Substituting (17)–(19) in equations (12)–(14) and collecting terms of different orders, as usual, one obtains a sequence of coupled ordinary differential equations.

For the zeroth order term,

$$f_0''' + f_0 f_0'' + \Lambda[1-(f_0')^2 + Bg_0^2] \pm A\lambda\theta_0 = 0, \tag{20}$$

$$g_0'' + f_0 g_0' - 2\Lambda f_0' g_0 = 0, \tag{21}$$

$$\theta_0'' + Pr f_0\theta_0' = 0 \tag{22}$$

with

$$\begin{aligned} f_0(\Lambda,0) = f_0'(\Lambda,0) = 0, \quad g_0(\Lambda,0) = \theta_0(\Lambda,0) = 1 \\ f_0'(\Lambda,\infty) = 1, \quad g_0(\Lambda,\infty) = \theta_0(\Lambda,\infty) = 0. \end{aligned} \tag{23}$$

For the first and higher order terms

$$f_1''' + f_0 f_1'' - 2(1+\Lambda) f_0' f_1' + 3 f_0'' f_1 + 2B\Lambda g_0 g_1 \pm A\lambda\theta_1 = \frac{\partial(f_0', f_0)}{\partial(\Lambda,\eta)}, \tag{24}$$

$$g_1'' + f_0 g_1' - 2f_0' g_1 - 2\Lambda(f_1' g_0 + g_1 f_0') + 3 f_1 g_0' = \frac{\partial(g_0, f_0)}{\partial(\Lambda,\eta)}, \tag{25}$$

$$Pr^{-1}\theta_1'' + f_0\theta_1' - 2f_0'\theta_1 + 3f_1\theta_0' = \frac{\partial(\theta_0, f_0)}{\partial(\Lambda,\eta)} \tag{26}$$

with

$$\begin{aligned} f_1(\Lambda,0) = f_1'(\Lambda,0) = g_1(\Lambda,0) = \theta_1(\Lambda,0) = 0 \\ f_1'(\Lambda,\infty) = g_1(\Lambda,\infty) = \theta_1(\Lambda,\infty) = 0 \end{aligned} \tag{27}$$

and

$$f_2''' + f_0 f_2'' - 2(2+\Lambda) f_0' f_2' + 5 f_0'' f_2 + 2B\Lambda g_0 g_2 \pm A\lambda\theta_2 = f_0' f_1' - f_0'' f_1, \tag{28}$$

$$g_2'' + f_0 g_2' - 4f_0' g_2 - 2\Lambda(g_0 f_2' + g_2 f_0') + 5 f_2 g_0' = f_0' g_1 - f_1 g_0', \tag{29}$$

$$Pr^{-1}\theta_2'' + f_0\theta_2' - 4f_0'\theta_2 + 5f_2\theta_0' = f_0'\theta_1 - f_1\theta_0' \tag{30}$$

with

$$\begin{aligned} f_2(\Lambda,0) = f_2'(\Lambda,0) = g_2(\Lambda,0) = \theta_2(\Lambda,0) = 0 \\ f_2'(\Lambda,\infty) = g_2(\Lambda\,\infty) = \theta_2(\Lambda,\infty) = 0. \end{aligned} \tag{31}$$

The local friction factor C_f and the local Nusselt number Nu are defined in [5] and now have the expressions

$$\tfrac{1}{2}C_f Re_R^{1/2} = \frac{r}{R}\left(\frac{U_e}{u_\infty}\right)^2 (2\xi)^{-1/2} \times \left[f_0''(\Lambda,0) + 2\xi\frac{d\Lambda}{d\xi} f_1''(\Lambda,0) + 4\xi^2\frac{d^2\Lambda}{d\xi^2} f_2''(\Lambda,0) + \cdots\right] \tag{32}$$

$$Nu\, Re_R^{-1/2} = -\frac{r}{R}\frac{U_e}{u_\infty}(2\xi)^{-1/2} \times \left[\theta_0'(\Lambda,0) + 2\xi\frac{d\Lambda}{d\xi}\theta_1'(\Lambda,0) + 4\xi^2\frac{d^2\Lambda}{d\xi^2}\theta_2'(\Lambda,0) + \cdots\right] \tag{33}$$

2.2. *Uniform surface heat flux*

In this case, the boundary conditions are

$$u = v = 0, \quad w = r\Omega, \quad q_w = -k\left(\frac{\partial T}{\partial y}\right)_y = 0 \quad \text{for } y = 0 \tag{34}$$

$$u = U_e, \quad v = w = 0, \quad T = T_\infty \quad \text{for } y \to \infty.$$

The transformations are the same as in Section 2.1 (i.e. UWT case) except equation (11) which is now replaced by

$$\theta(\xi,\eta) = [T(x,y) - T_\infty] Re_R^{1/2}/(q_w R/k). \tag{35}$$

The governing equations are the same as (20)–(31) with the replacement of λ by λ^* where

$$Gr^* = a\beta q_w R^4/k\nu^2 \quad \text{and} \quad \lambda^* = Gr^*/Re_R^{5/2}. \tag{36}$$

For this case, the Nusselt number has the expression

$$Nu\, Re_R^{-1/2} = \left[\theta_0'(\Lambda,0) + 2\xi \frac{d\Lambda}{d\xi}\theta_1(\Lambda,0) + 4\xi^2 \frac{d^2\Lambda}{d\xi^2}\theta_2(\Lambda,0) + \cdots \right]^{-1}. \quad (37)$$

3. NUMERICAL RESULTS AND CONCLUSIONS

Governing equations (20)–(22), (24)–(26) and (28)–(30) with their boundary conditions (23), (27) and (31) respectively can be treated as simultaneous ordinary differential equations with Λ, B, A, λ and Pr regarded as parameters for the UWT case. However, for the UHF case λ is replaced by λ^*. They have been numerically integrated by the multiple shooting method using the subroutine DTPTB [15] from the International Mathematical and Statistical Library on DEC-System 10.

3.1. *Uniform wall temperature case*

The velocity and temperature wall derivatives are given in Tables 1, 2 3 and 4 for $B = 1, 4, 10$; $Pr = 0.7, 1.0$ and $\lambda = -2.0, 0, 0.5, 1.0$. Knowing the values of various f_i, g_i and θ_i, the significant boundary-layer quantities, such as the local frictional coefficient and the local Nusselt number are obtained using the formulae (32) and (33). When $\lambda = 0$, our problem reduces to that of Lee [5], which was used as a check on our calculations and the agreement was found to be fairly good. For comparison of our results with those of Lee [5], his curves ($\lambda = 0$) are depicted by broken lines in our figures.

Results for velocity distributions are shown in Figs. 1, 2 and 5. For aiding flow, at the stagnation point, it can be seen (Fig. 5) that the velocity gradient at the wall increases as the buoyancy force increases and hence δ_v decreases. Comparison of Figs. 1, 2 and 5, for $B = 1$, shows the influence of buoyancy on δ_v, i.e. the boundary-layer thickness decreases rapidly as the angle increases. For $B = 10$ (Figs. 1 and 2), the velocity gradient at the wall increases as the buoyancy force increases with an accompanying increase in the velocity near the wall region. In the case of non-rotating mixed convection flow [11], overshooting beyond the local free stream velocity is observed in the vicinity of $\lambda = 5$ (and above). In the case of flow due to a rotating sphere, for a given buoyancy force, overshooting takes place earlier. This is due to coupling between buoyancy and rotation which enhance each other resulting in increased overshooting of the velocity profiles.

The temperature distributions are displayed in Fig. 5 (for $\Lambda = 0.5$) and Fig. 6 (for $\Lambda = 0.1$). It is obvious that the thermal boundary-layer thickness, δ_θ, decreases and hence the temperature gradient at wall increases as the buoyancy force increases. In absence of forced flow, it is clear from Suwono's work [6] that the temperature gradient increases as λ increases. However, from the

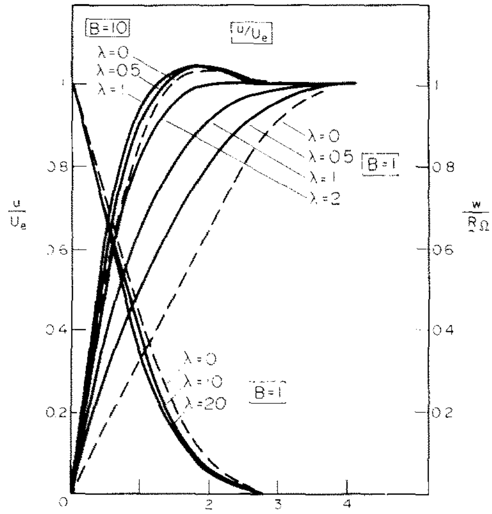

FIG. 1. u/U_e and $W/R\Omega$ vs η for $B = 1$, 10 and $Pr = 1$ when $\Lambda = 0.1$.

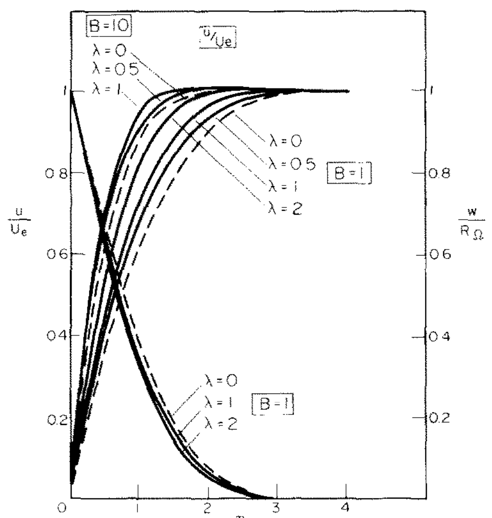

FIG. 2. u/U_e and $W/R\Omega$ vs η for $B = 1$, 10 and $Pr = 1$ when $\Lambda = 0.3$.

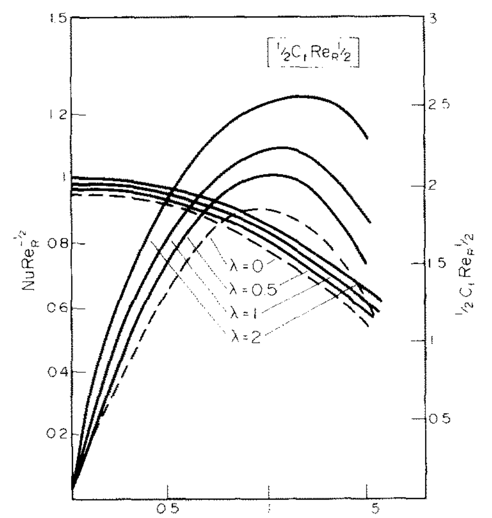

FIG. 3. Angular distributions of the local friction factor and the local Nusselt number for $B = 1$ and $Pr = 1$.

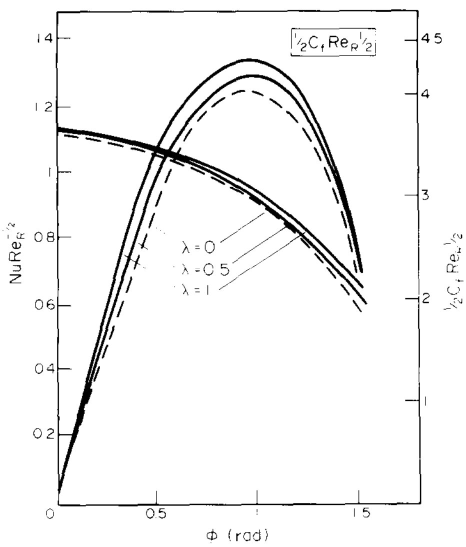

FIG. 4. Angular distributions of the local friction factor and the local Nusselt number for $B = 10$ and $Pr = 1$.

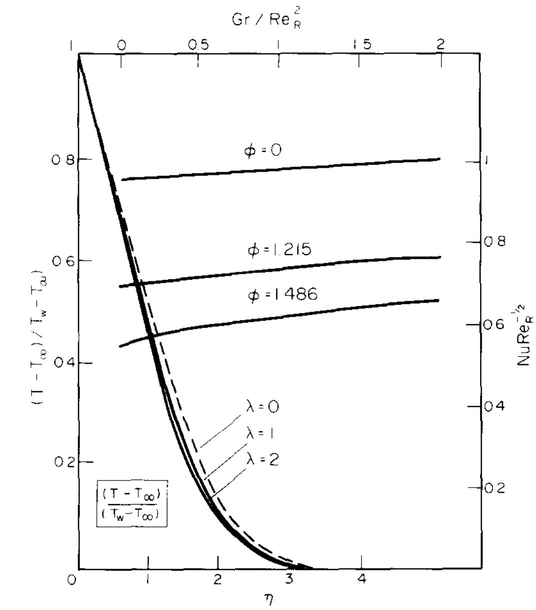

FIG. 6. Temperature profiles when $\Lambda = 0.1$ and heat transfer results at representative angular positions for $B = 1$, $Pr = 1$.

present work, it is observed that the uniform flow from infinity decreases the steepness of the temperature profiles.

The angular distributions of the local wall shear stress, $\frac{1}{2}C_f Re_R^{1/2}$, for the local force stream velocity distributions are shown in Figs. 3 and 4 for $B = 1$ and 10 respectively. The local wall shear increases with buoyancy force and rotation. However, in comparison with buoyancy, rotation has a more pronounced effect on wall shear.

The eruption point of flow can be determined by finding the point where the x-component of local-wall frictional stress has the same magnitude but with the opposite direction. An increase in the rotation

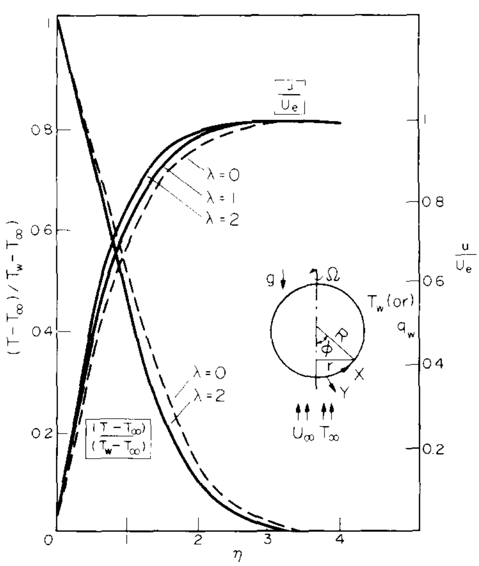

FIG. 5. Velocity profiles when $\Lambda = 0.5$ and temperature profiles when $\Lambda = 0.3$ for $B = 1$, $Pr = 1$.

parameter, B, can be interpreted in two ways: either decrease in the free stream velocity, u_∞, or the increase in the rotation speed, Ω.

According to Suwono [6], for sufficiently large values of λ, the separation occurs not due to collision of flow but due to the vanishing of the local stream stress at the wall. The present work is a generalization of Suwono's [6] problem, wherein the effect of free stream velocity is taken into account. Now, consider the case when the buoyancy parameter, λ, has a fixed value. From Figs. 3 and 4, it is clear that the curves for wall shear stress become steeper as B increases, which results in shifting of the separation point towards the equator. The imposition of a uniform flow from infinity on the flow due to rotation results in delaying the flow separation. Thus for sufficiently large values of u_∞, it is possible that the separation occurs due not to collision but due to the vanishing of the local wall shear stress at wall.

When Ω and u_∞ are fixed, the increase in buoyancy force increases the local wall shear with a resulting delay in the flow separation. This is because inside the boundary layer, the buoyancy force assists the resultant flow due to forced flow from infinity, u_∞, and the rotation.

The local surface heat transfer rate increases as λ increases (Figs. 3 and 4) for aiding flow, while an opposite trend is observed for opposing flow. Also for a given buoyancy force, the local Nusselt number is seen to decrease with increasing angle from the stagnation point. To provide a better understanding of the local heat transfer characteristics for the entire regime of mixed convection for aiding flow, Fig. 6 has been drawn to show the effect of buoyancy force on the local Nusselt

Table 1. Wall derivatives of functional coefficients for $B = 1$, $Pr = 1$ and λ ranging from 0 to 1 (UWT case)

ϕ	λ	$f''_0(0)$	$-f''_1(0) \times 10$	$f''_2(0) \times 10^2$	$-g'_0(0)$	$g'_1(0) \times 10$	$-g'_2(0) \times 10^2$	$-\theta'_0(0)$	$-\theta'_1(0) \times 10^2$	$\theta'_2(0) \times 10^2$
0	0	1.11295	0.455269	0.434428	0.784928	0.484930	0.594232	0.553923	0.465207	0.115101
	0.5	1.17999	0.242397	0.191980	0.796772	0.441912	0.535561	0.561318	0.502115	0.104833
	1	1.24575	0.036227	−0.045849	0.808051	0.400749	0.477901	0.568377	0.557988	0.099862
0.474	0	1.09382	0.474595	0.460724	0.774630	0.498041	0.616627	0.552084	0.447402	0.112740
	0.5	1.11668	0.259041	0.212939	0.787484	0.455923	0.558519	0.580210	0.490570	0.103689
	1	1.12383	−0.051187	−0.029174	0.799667	0.415829	0.501600	0.567929	0.553905	0.100315
0.951	0	1.01396	0.566555	0.589950	0.732111	0.556869	0.719462	0.544094	0.351877	0.337309
	0.5	1.11097	0.330203	0.315201	0.748934	0.517061	0.664806	0.555303	0.427707	0.219163
	1	1.20513	0.107097	0.039525	0.764558	0.480087	0.606977	0.565741	0.527636	0.119718
1.215	0	0.90520	0.727876	0.830436	0.675535	0.648304	0.887092	0.532306	0.149375	0.063818
	0.5	1.03371	0.442896	0.468813	0.697388	0.610026	0.825403	0.547992	0.293806	0.073534
	1	1.15683	0.184015	0.136681	0.717064	0.576007	0.768651	0.562165	0.462497	0.091149
1.486	0	0.642531	1.397090	1.947340	0.546996	0.926041	1.455710	0.498525	−0.979418	−0.171601
	0.5	0.848755	0.856326	1.143400	0.580533	0.889511	1.361370	0.527778	−0.405154	−0.066352
	1	1.037850	0.438609	0.529878	0.607994	0.863309	1.295130	0.551806	0.092891	0.021849

Table 2. Wall derivatives of functional coefficients for $B = 4$, $Pr = 1$ and $\lambda = 0, 1$ (UWT case)

ϕ	λ	$f''_0(0)$	$-f''_1(0) \times 10$	$f''_2(0) \times 10^2$	$-g'_0(0)$	$g'_1(0) \times 10$	$-g'_2(0) \times 10^2$	$-\theta'_0(0)$	$-\theta'_1(0) \times 10^2$	$\theta'_2(0) \times 10^2$
0	0	1.62326	0.430797	0.229157	0.846309	0.447165	0.498493	0.589935	0.132447	0.266384
	1.0	1.74130	0.080887	−0.155502	0.864461	0.378328	0.409345	0.601508	0.142419	0.253918
0.474	0	1.59085	0.451937	0.254263	0.834517	0.459146	0.518155	0.587746	0.131507	0.266307
	1	1.71947	0.098307	−0.138254	0.854231	0.393644	0.432470	0.600460	0.141859	0.254872
0.951	0	1.45484	0.591977	0.419391	0.785675	0.520170	0.618427	0.578057	0.128092	0.268887
	1	1.62618	0.204485	−0.026090	0.811585	0.460190	0.537879	0.595610	0.140455	0.260611
1.215	0	1.26745	0.841333	0.746304	0.72021	0.615464	0.785395	0.563223	0.113320	0.252238
	1	1.49549	0.374229	0.180227	0.754145	0.561376	0.708058	0.587887	0.131651	0.253598
1.486	0	0.799354	2.03432	2.59105	0.567674	0.918675	1.40764	0.516344	−0.018074	−0.009604
	1	1.117301	1.08776	1.24744	0.622111	0.877019	1.30302	0.564013	0.051070	0.103839

Table 3. Wall derivatives of functional coefficients for $B = 10$, $Pr = 1$ and λ ranging from 0 to 1 (UWT case)

ϕ	λ	$f_0''(0)$	$-f_1''(0)\times 10$	$f_2''(0)\times 10^3$	$-g_0'(0)$	$g_1'(0)\times 10$	$-g_2'(0)\times 10^2$	$-\theta_0'(0)$	$-\theta_1'(0)\times 10$	$\theta_2'(0)\times 10^2$
	0	2.52162	0.473325	0.490032	0.936157	0.436351	0.435593	0.643358	0.218541	0.421552
0	0.5	2.57275	0.334820	−0.959479	0.942832	0.410176	0.403630	0.647720	0.223935	0.417759
	1	2.62353	0.202387	−2.35768	0.949358	0.384242	0.371768	0.651986	0.229858	0.415723
	0	2.46636	0.514244	0.88956	0.922345	0.450573	0.456818	0.640726	0.219214	0.426125
0.474	0.5	2.52218	0.373505	−0.59628	0.929623	0.425122	0.425764	0.645532	0.224560	0.422164
	1	2.57756	0.239096	−2.02825	0.936722	0.399952	0.394810	0.650221	0.230454	0.420076
	0	1.91109	1.11531	7.81679	0.787472	0.618729	0.729578	0.610173	0.207237	0.438968
1.215	0.5	2.01203	0.918736	5.54694	0.800617	0.597581	0.704197	0.619864	0.213715	0.433972
	1	2.11115	0.730052	3.34933	0.813083	0.578089	0.679503	0.629060	0.220607	0.432144
	0	1.08732	3.16731	37.8068	0.601712	0.958318	1.41623	0.545761	0.048914	0.146015
1.486	0.5	1.26316	2.66678	30.9797	0.625937	0.940993	1.38248	0.567039	0.070775	0.169954
	1	1.43013	2.24778	25.2600	0.647179	0.926946	1.35280	0.585725	0.093727	0.200476

Table 4. Wall derivatives of functional coefficients at the stagnation point for $B = 1, 10$, $Pr = 0.7$ and λ ranging from -2 to 1 (UWT case)

B	λ	$f_0''(0)$	$-f_1''(0)\times 10$	$f_2''(0)\times 10^2$	$-g_0'(0)$	$g_1'(0)\times 10$	$-g_2'(0)\times 10^2$	$-\theta_0'(0)$	$-\theta_1'(0)\times 10^2$	$\theta_2'(0)\times 10^2$
1	0	1.11295	0.455269	0.434428	0.784928	0.484930	0.594232	0.484007	1.41950	0.255175
	1	1.25518	−0.028864	−0.136551	0.810716	0.376982	0.440758	0.497159	0.830813	0.128657
	−2	2.29818	1.09179	0.671132	0.903775	0.573068	0.587498	0.536537	4.20427	0.785461
10	0	2.52162	0.473325	0.049003	0.936157	0.436351	0.435593	0.554226	3.46718	0.585365
	1	2.63091	0.166688	−0.278844	0.951124	0.371031	0.353733	0.562418	3.21884	0.515544

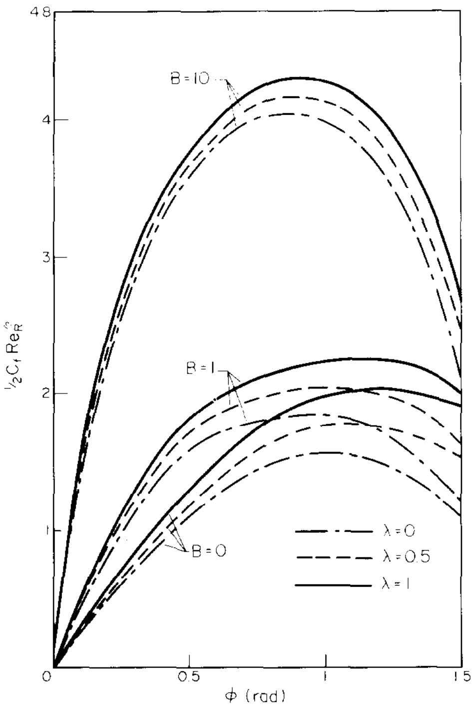

FIG. 7. Angular distributions of the local friction factor for $B = 0, 1, 10$ and $Pr = 1$ (UHF case).

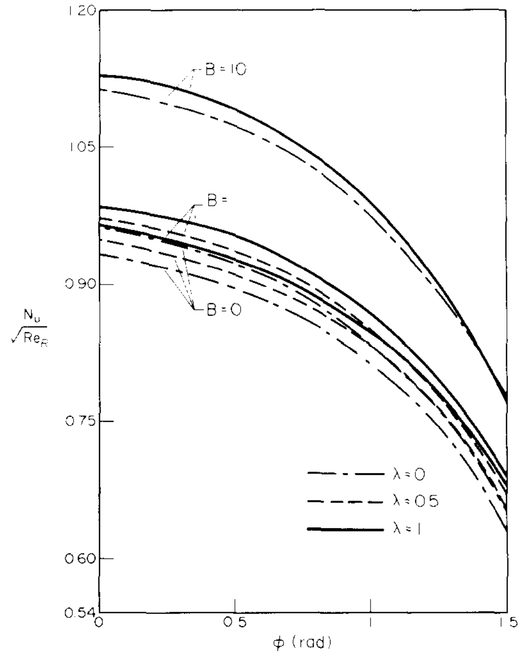

FIG. 8. Angular distribution of the local Nusselt number for $B = 0, 1, 10$ and $Pr = 1$ (UHF case).

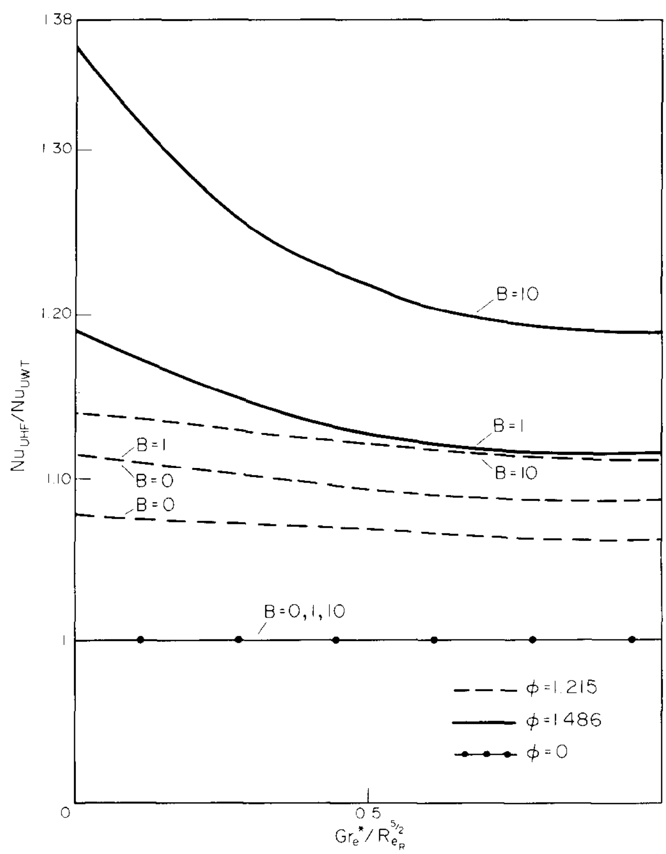

FIG. 9. A comparison of the local Nusselt numbers between uniform surface heat flux and uniform wall temperature.

number at three representative angular positions 0, 1.215 and 1.486.

The asymptote at the stagnation point for the pure forced convection (i.e. a uniform flow from infinity) about a non-rotating sphere (Chen and Mucoglu [11]) is $Nu\ Re_R^{-1/2} = 0.8149$. In our case, $Nu\ Re_R^{-1/2} = 0.8383, 0.9599$ for $B = 1, 10$ respectively. Thus, the rotation enhances the heat transfer rate at the stagnation point which is as expected. The same trend may be expected to hold as the angle is increased.

3.2. *Uniform surface heat flux case*

Numerical computations were carried out for $Pr = 1$; $B = 0, 1, 10$; and for various values of buoyancy parameter λ^*. When $B = 0$, our problem is comparable with [14] (wherein $Pr = 1$ has been taken instead of $Pr = 0.7$). According to them both the local wall shear stress and the local Nusselt number increase with buoyancy for assisting flow.

As in the case of UWT, for a fixed λ^* (from Figs. 7 and 8), it is clear that as B increases both $\frac{1}{2}C_f Re_R^{1/2}$ and $Nu\,Re_R^{-1/2}$ increase and the curves for wall shear stress become steeper which results in shifting of the separation point towards the equator. Thus for sufficiently large values of Ω, it is possible that the separation occurs due to collision of flow. Also for a fixed B, increase in buoyancy force increases the local wall shear with a resulting delay in the flow separation.

Next, we compare the local Nusselt number results for UHF case with those for UWT case. This can be done as in [12] by defining an equivalent buoyancy parameter λ_e between the two cases. This leads one to the result

$$\frac{Nu_{\mathrm{UHF}}}{Nu_{\mathrm{UWT}}} = -\frac{2}{3}\frac{\sqrt{2+\cos\phi}}{(1+\cos\phi)}\cdot\frac{1}{\theta(\Lambda,0)}\cdot\frac{1}{\theta'(\Lambda,0)}, \quad (38)$$

where θ, θ' values are taken from UHF and UWT cases, respectively.

The Nusselt number ratio versus λ_e is illustrated in Fig. 9 at representative angular positions of $\phi = 0$, 1.215 and 1.486 for the rotation parameter $B = 0, 1, 10$. It is seen (Fig. 9) that $Nu_{\mathrm{UHF}}/Nu_{\mathrm{UWT}}$ ratio is unity for $\phi = 0$ and increases as ϕ increases. Thus for an equivalent buoyancy force effect, heating by uniform surface heat flux yields larger local Nusselt number than heating by uniform wall temperature. Also the ratio $Nu_{\mathrm{UHF}}/Nu_{\mathrm{UWT}}$ is larger for the rotating sphere (in comparison with the non-rotating case [14]) and further this ratio increases as B increases. Thus, even though rotation enhances the heat transfer rate in both cases, the effect is more pronounced in the UHF case than by UWT case.

The effect of variation of Prandtl number on the flow and heat transfer due to buoyancy, rotation and forced flow has not been considered in this paper and this could be a subject matter for further investigation.

REFERENCES

1. W. H. H. Banks, The laminar boundary layer on a rotating sphere, *Acta mech.* **24**, 273–287 (1976).
2. L. A. Dorfman and A. Z. Serazetdinov, Laminar flow and heat transfer near rotating axisymmetric surface, *Int. J. Heat Mass Transfer* **8**, 317–327 (1965).
3. L. A. Dorfman and V. A. Mironova, Solutions of equations for the thermal boundary layer at rotating axisymmetric surface, *Int. J. Heat Mass Transfer* **13**, 81–92 (1970).
4. B. T. Chao and R. Greif, Laminar forced convection over rotating bodies, *ASME J. Heat Transfer* **96**, 463–466 (1974).
5. M. H. Lee, D. R. Jeng and K. J. De Witt, Laminar boundary layer transfer over rotating bodies in forced flow, *ASME J. Heat Transfer* **100**, 496–502 (1978).
6. A. Suwono, Buoyancy effects on flow and heat transfer on rotating axisymmetric round-nosed bodies, *Int. J. Heat Mass Transfer* **23**, 819–831 (1980).
7. E. M. Sparrow and J. L. Gregg, Buoyancy effects in forced convection flow and heat transfer, *J. appl. Mech.* **81**, 133–134 (1959).
8. A. A. Szewezyk, Combined forced and free convection laminar flow, *J. Heat Transfer* **86**, 501–507 (1964).
9. J. H. Merkin, The effect of buoyancy forces on the boundary layer flow over a semi-infinite vertical flat plate in a uniform free stream, *J. Fluid Mech.* **35**, 439–450 (1969).
10. T. S. Chen and A. Mucoglu, Buoyancy effects on forced convection along a vertical cylinder, *J. Heat Transfer* **97**, 198–203 (1975).
11. T. S. Chen and A. Mucoglu, Analysis of mixed forced and free convection about a sphere, *Int. J. Heat Mass Transfer* **20**, 867–875 (1977).
12. H. J. Merk, Rapid calculations for boundary layer transfer for wedge solutions and asymptotic expansions, *J. Fluid Mech.* **5**, 460–480 (1959).
13. B. T. Chao and R. O. Fagbenle, On Merk's method of calculating boundary layer transfer, *Int. J. Heat Mass Transfer* **17**, 223–240 (1974).
14. T. S. Chen and A. Mucoglu, Mixed conversion about a sphere with uniform surface heat flux, *ASME J. Heat Transfer* **100**, 542–544 (1978).
15. Solve a System of Ordinary Differential Equations with Two-point Boundary Conditions Using Multiple Shooting Method, Subroutine DTPTB, IMSL (June 1980).

CONVECTION MIXTE AUTOUR D'UNE SPHERE TOURNANTE

Résumé—On présente une analyse théorique de l'écoulement et du transfert thermique et des effets de la gravité sur la couche limite laminaire sur une sphère tournante placée dans un écoulement forcé, avec deux espèces de conditions : température pariétale uniforme et flux surfacique uniforme. En appliquant des transformations de coordonnées appropriées et en utilisant des séries du type Merk, les équations de quantité de mouvement et d'énergie sont réduites à un système d'équations différentielles couplées, qui dépendent des paramètres de rotation et de gravité. Des calculs numériques sont faits pour des nombres de Prandtl 0,7 et 1,0 et pour différentes valeurs des paramètres de rotation et de gravité. Pour l'écoulement aidé, on trouve que le coefficient de frottement et le nombre de Nusselt local augmentent avec les forces de gravité. La vitesse locale de l'écoulement libre augmente avec la gravité qui, en retour, affecte le coefficient de frottement et le nombre de Nusselt. Le couplage entre rotation et gravité augmente l'excès de vitesse des profils de vitesse au voisinage de la sphère. Pour un effet de gravité équivalent, le chauffage à flux surfacique constant conduit à des nombres de Nusselt locaux plus importants que pour le chauffage à température pariétale uniforme. Le rapport Nu_{UHF}/Nu_{UWT} est plus grand pour la sphère tournante (en comparaison du cas sans rotation) et le rapport croît lorsque la sphère tourne plus vite. On examine l'effet de l'écoulement libre, de la rotation et de la gravité sur l'éruption de l'écoulement et on fait une suggestion pour une étude ultérieure.

MISCHKONVEKTION AN EINER ROTIERENDEN KUGEL

Zusammenfassung—Dieser Artikel stellt eine theoretische Untersuchung der Einflüsse einer Auftriebskraft auf eine laminare Grenzschicht an einer in erzwungener Strömung rotierenden Kugel unter zwei Arten von Heizbedingungen vor: konstante Wandtemperatur und konstante Wärmestromdichte an der Oberfläche. Durch Anwendung von entsprechenden Koordinatentransformationen und Benutzung der Merk'schen Reihen werden die Erhaltungsgleichungen für Impuls und Energie auf ein System von gekoppelten gewöhnlichen Differentialgleichungen reduziert. Numerische Berechnungen wurden für Prandtl-Zahlen von 0,7, 1,0 und für verschiedene Werte der Auftriebs- und Rotationsparameter durchgeführt. Für eine gleichgerichtete Strömung ergab sich, daß der Reibungsfaktor und die örtliche Nusselt-Zahl mit größer werdender Auftriebskraft zunehmen. Die örtliche freie Strömungsgeschwindigkeit wird mit dem Auftrieb größer, was wiederum den Reibungskoeffizienten und die Nusselt-Zahl beeinflußt. Die Kopplung zwischen Rotation und Auftrieb zeigt sich in einem zunehmenden Überschwingen der Geschwindigkeitsprofile in der Nähe der rotierenden Kugel. Für den gleichen Auftriebseffekt führt das Heizen mit konstanter Wärmestromdichte an der Oberfläche zu einer größeren Nusselt-Zahl als das Heizen bei konstanter Wandtemperatur. Das Verhältnis von Nu_{UHF}/Nu_{UWT} ist größer für eine rotierende Kugel (verglichen mit dem nichtrotierenden Fall), und außerdem steigt dieses Verhältnis an, wenn die Kugel sich schneller dreht. Es wurde der Einfluß von freier Strömung, Rotation und Auftrieb auf die Strömungsablösung untersucht. Außerdem wird ein Vorschlag für weitere Untersuchungen gemacht.

СМЕШАННАЯ КОНВЕКЦИЯ ОКОЛО ВРАЩАЮЩЕЙСЯ СФЕРЫ

Аннотация—В работе представлен теоретический анализ течения и характеристик теплообмена с учетом влияния массовой силы на ламинарный пограничный слой над вращающейся в вынужденном потоке сферой при двух видах тепловых условий: однородная температура стенки и однородный на поверхности тепловой поток. При применении существующих преобразований координат и использовании рядов Мерка уравнения сохранения энергии и движения сводятся к связанной системе обычных дифференциальных уравнений, зависящих от параметров вращения и массовой силы и угла между ними. Численные расчеты выполнены для чисел Прандтля 0,7; 1,0 и различных значений параметра вращения и подъемной силы. Найдено, что для вторичного течения как коэффициент трения, так и локальное число Нуссельта возрастают с увеличением подъемной силы. Локальная скорость свободноконвективного потока растет с подъемной силой, которая, в свою очередь, влияет на коэффициент трения и число Нуссельта. Взаимодействие вращения и подъемной силы приводит к росту отклонения профилей скорости вблизи вращающейся сферы. При эквивалентных подъемных силах нагрев однородным поверхностным тепловым потоком дает бóльшее локальное число Нуссельта, чем нагрев при однородной температуре стенки. Отношение Nu_{UHF}/Nu_{UWT} выше для вращающейся сферы (по сравнению со случаем невращающейся) и в дальнейшем отношение растет с ускорением вращения. Исследованы влияние свободного потока, вращения и массовой силы на подъем течения и даны предложения по дальнейшему исследованию.